Processivity of Chimeric Class V Myosins*

Elena B. Krementsova[1]**, Alex R. Hodges**[1]**, Hailong Lu**[1]**, and Kathleen M. Trybus**[2]
From the Department of Molecular Physiology and Biophysics, University of Vermont, Burlington, Vermont 05405

Unconventional myosin V takes many 36-nm steps along an actin filament before it dissociates, thus ensuring its ability to move cargo intracellularly over long distances. In the present study we assessed the structural features that affect processive run length by analyzing the properties of chimeras of mouse myosin V and a non-processive class V myosin from yeast (Myo4p) (Reck-Peterson, S. L., Tyska, M. J., Novick, P. J., and Mooseker, M. S. (2001) *J. Cell Biol.* 153, 1121–1126). Surprisingly a chimera containing the yeast motor domain on the neck and rod of mouse myosin V (Y-MD) showed longer run lengths than mouse wild type at low salt. Run lengths of mouse myosin V showed little salt dependence, whereas those of Y-MD decreased steeply with ionic strength, similar to a chimera containing yeast loop 2 in the mouse myosin V backbone. Loop 2 binds to acidic patches on actin in the weak binding states of the cycle (Volkmann, N., Liu, H., Hazelwood, L., Krementsova, E. B., Lowey, S., Trybus, K. M., and Hanein, D. (2005) *Mol. Cell* 19, 595–605). Constructs containing yeast loop 2, which has no net charge compared with +6 for wild type, showed a higher K_m for actin in steady-state ATPase assays. The results imply that a positively charged loop 2 and a high affinity for actin are important to maintain processivity near physiologic ionic strength.

Unconventional myosin V is an actin-based motor protein involved in organelle and mRNA transport as well as membrane trafficking (for a review, see Ref. 1). Each head of dimeric myosin V consists of a motor domain that binds actin and hydrolyzes ATP followed by an ~24-nm neck region that binds six calmodulins (CaMs).[3] The coiled-coil rod formed by both heavy chains ends in a globular cargo-binding domain. It has been clearly established that myosin V motors from vertebrates are processive, which allows a single motor to transport cargo, in 36-nm steps, for several micrometers along an actin filament (2).

Several kinetic and structural adaptations allow myosin V to be processive. The rate-limiting step for myosin V is ADP release, ensuring that it spends most of its time bound to actin in a strong binding state. In contrast, non-processive myosin II spends most of its ATPase cycle detached from actin in a weak binding state (for a review, see Ref. 3). Long processive runs require that there must be communication between the two heads to ensure that at least one head is bound to the actin filament at all times. Recent evidence favors the idea that this coordination is achieved by intramolecular strain between the heads

(4–7). Finally it is thought that a high affinity for actin in the weak binding states (ATP and ADP·P_i) is favorable for processivity by helping to maintain actin and myosin in proximity. Myosin V has a substantially stronger affinity for actin in the weak binding states than myosin II (8). In the widely accepted hand-over-hand mechanism of walking (for a review, see Ref. 9), the rear head detaches upon binding ATP, allowing the attached head to undergo its powerstroke. The detached head then swings forward as it hydrolyzes ATP and finds the next actin binding site via a diffusive search. A high affinity for actin may help ensure that the binding of the new lead head is faster than the rate at which the attached head dissociates from actin, allowing a processive run to continue.

Not all class V myosins are processive. A recent kinetic analysis of *Drosophila* myosin V concluded that it is not a processive motor (10). The two class V myosins from the yeast *Saccharomyces cerevisiae* (Myo2p and Myo4p) have been reported to be non-processive based on several indirect assays (11). Accordingly we engineered and expressed chimeras of processive murine myosin V and non-processive yeast myosin V (Myo4p) to further define the structural and functional features that contribute to processive movement. Surprisingly we showed that the yeast motor domain on the neck and rod of murine myosin V has the potential to drive processive motion to an even greater extent than the wild-type mouse construct. We also showed that the net charge of loop 2, a region implicated in the initial weak interaction between myosin and actin (12–15), affects run lengths by virtue of its ability to strengthen the weak binding steps in the ATPase cycle. We conclude that a myosin optimized for long runs at physiologic ionic strength should have a highly positively charged loop 2.

MATERIALS AND METHODS

Myosin V Constructs—The constructs described below contained yellow fluorescent protein (YFP) followed by a FLAG epitope (DYKD-DDDK) at the C terminus to facilitate purification. Constructs were cloned into pAcSG2 (BD Biosciences) for production of recombinant baculovirus. The wild-type (WT) murine myosin V HMM construct was truncated at amino acid 1098 (16). A yeast motor domain chimera (Y-MD) was created by exchanging yeast Myo4P motor domain into the WT-HMM-YFP backbone. The plasmid pYC352-MYO4 (a gift from Brian Haarer and Karen Beningo) was used as the PCR template for this construct. To exchange motor domains, two XhoI sites in WT-HMM-YFP were ablated, and a new one was engineered at Leu-759/Glu-760. The Myo4p clone was also modified. Myo4p motor domain was cloned into pCR4-TOPO using PCR primers that contained an NcoI site followed by an Ala, 5′-GAACCATGGCATTTGAAGTAGGAACTAA-G-3′ (forward), and a XhoI site, 5′-GAGGCTCGAGAAATGCAAGC-ATTCCTGCTTTAAAG-3′ (reverse). Then an XhoI site at Ala-310 and an NcoI site at Pro-673 sites were ablated (plasmid name, TOPO-MYO4md). Both plasmids (WT and TOPO-MYO4md) were digested with NcoI and XhoI, and the Myo4p motor domain fragment was cloned into the WT backbone. To exchange yeast (Myo4p) loop 2 into the mouse motor domain a SacI site was created at the N terminus of loop 2 and an EcoRI site was created at the C terminus. The Myo4p loop 2 was synthesized by PCR with added SacI and EcoRI sites. The

[1] These authors contributed equally to this work.
[2] To whom correspondence should be addressed: Dept. of Molecular Physiology and Biophysics, University of Vermont, 149 Beaumont Ave., Burlington, VT 05405. Tel.: 802-656-8750; Fax: 802-656-0747; E-mail: kathleen.trybus@uvm.edu.
[3] The abbreviations used are: CaM, calmodulin; Y-MD, a chimera containing the motor domain of yeast class V myosin (Myo4p) and the neck and rod of mouse myosin V; Y-Loop2, a chimera containing loop 2 from yeast class V myosin (Myo4p) in the mouse myosin V backbone; WT, mouse wild-type; TIRF, total internal reflection fluorescence; YFP, yellow fluorescent protein; HMM, heavy meromyosin; DTT, dithiothreitol.

sequence of the region flanking loop 2 was FQD (mouse)-ELRS . . . TLG (yeast)-HQFR (mouse). The boundaries of loop 2 were defined from a sequence alignment of chicken, mouse, and the two yeast class V myosins.

Protein Purification of Expressed HMMs—Sf9 cells were infected with recombinant viruses for the heavy chain and for CaM and incubated for ~72–75 h at 27 °C. CaMΔall, a calmodulin mutant lacking all calcium binding sites, was used to ensure complete occupancy of the IQ motifs. Cells were pelleted and resuspended in 10 mM imidazole, pH 7.4, 0.3 M NaCl, 1 mM EGTA, 2 mM DTT, 25 μg/ml CaMΔall, and protease inhibitors (0.5 mM 4-(2-aminoethyl)benzenesulfonyl fluoride, 5 μg/ml leupeptin, 0.78 mg/ml benzamidine). The cells were lysed by sonication, and the lysate was centrifuged for 15 min at 250,000 × g in the presence of 2 mM MgATP. Following incubation with FLAG affinity resin (Sigma) for 30 min, the resin was sedimented for 5 min at 1000 rpm and washed with buffer (10 mM imidazole, pH 7.4, 0.3 M NaCl, 1 mM EGTA), and the bound protein was eluted using a 0.1 mg/ml solution of FLAG peptide in the same buffer. Fractions were pooled, concentrated in 50% glycerol, and stored at −20 °C.

Preparation of Calmodulin and Actin—CaMΔall, a calmodulin mutant lacking all calcium binding sites (E31Q,E67Q,E104Q,E140Q), was expressed and purified essentially as described previously (16). CaMΔall was cloned into pVL1393 vector for baculovirus expression and into pNew, a pT7-7-based plasmid, for bacterial expression. The cell pellet was resuspended in 50 mM Tris-Cl, pH 7.5, 2 mM EDTA, 0.5 mM 4-(2-aminoethyl)benzenesulfonyl fluoride, 1 μg/ml leupeptin, 1 mM DTT. After sonication, the solution was clarified for 15 min at 26,000 × g. The supernatant was boiled for 5 min, clarified, and loaded onto a DEAE-Sephacel column (10 ml of resin/0.5-liter culture) equilibrated in buffer A (50 mM Tris-Cl, pH 7.5, 2 mM EDTA, 1 mM DTT). The column was washed first with buffer A and then with buffer A with 0.1 M NaCl. CaM was eluted with 10 volumes of a linear salt gradient from 100 to 300 mM NaCl. Protein was concentrated and stored in 50% glycerol at −20 °C. Chicken skeletal actin was prepared from acetone powder essentially as described previously (17).

Processivity Assay by Single Molecule Total Internal Reflection Fluorescence (TIRF) Microscopy—Single molecule motility assays using TIRF microscopy were performed essentially as described before with the exception that Alexa 660-phalloidin-labeled actin filaments were immobilized onto the cover glass with N-ethylmaleimide-modified myosin instead of via biotin-streptavidin linkage (18). For all TIRF, motility, and landing rate assays, the myosin V constructs at 0.2 mg/ml were mixed with a 2-fold molar excess of actin and 1 mM MgATP and centrifuged for 20 min at 400,000 × g to remove myosin that was unable to dissociate from actin in the presence of ATP. For TIRF assays, flow cells were first incubated with 0.1 mg/ml N-ethylmaleimide-modified myosin for 2 min, rinsed, incubated with 0.5 μM Alexa 660-phalloidin-labeled actin filaments for 2 min, and then rinsed with Motility Buffer. Motility Buffer contained 25 mM imidazole, pH 7.1, 4 mM MgCl₂, 1 mM EGTA, 10 mM DTT, an oxygen-scavenging system (3 mg/ml glucose, 0.1 mg/ml glucose oxidase, 0.18 mg/ml catalase), an ATP-regenerating system (0.5 mM phosphoenolpyruvate and 100 units/ml pyruvate kinase), 0.1 mg/ml CaMΔall, and varying concentrations of MgATP and KCl. The final assay buffer consisted of Motility Buffer with 0.5 mg/ml bovine serum albumin, 50 μM MgATP, and 25–100 mM KCl. The ATPase rate of Y-MD is only about half-maximal at 50 μM MgATP, whereas WT and Y-Loop2 are close to maximal at this ATP concentration (data not shown). The myosin V concentration was 0.5–1.0 nM. The assay was performed at room temperature (25 ± 1 °C) on a Nikon TE2000-U microscope equipped with a PlanApo objective lens (×100;

numerical aperture, 1.45) for through-the-objective TIRF microscopy. The 488-nm line of an argon laser (Spectra-Physics model 163) was used to excite the YFP-tagged myosin molecules for visualization through a Chroma HQ 560/80 filter (Chroma Technology, Brattleboro, VT). The camera was an image-intensified digital charge-coupled device camera (DVC Intensicam IV S, Austin, TX). The final pixel resolution was 21.5 nm. It was necessary to use a 166-ms exposure time to obtain high quality images of the YFP-labeled myosins. At this setting, the controlling software (QEDInVivo, Media Cybernetics, Inc., Silver Spring, MD) limited the frame rate to 3.4 frames/s.

A data set consists of a sequence of images showing single myosin molecules moving processively along actin filaments. The image sequence was processed by a custom program that tracked the movement of each myosin molecule through successive frames. For each run, the program generated a trajectory and calculated the run length (the distance a single myosin travels from its initial attachment to the filament to its dissociation). Each trajectory was then played back and verified manually. We required that each myosin move continuously for at least four frames to qualify as a run. This was necessary to distinguish between directed movement and Brownian motion. With a frame rate of 3.4 frames/s, the total time for each frame is 0.3 s, or 1.2 s for four frames. However, the time interval between the midpoint of four frames is 0.9 s. The shutter is open for 166 ms of the 0.3 s during which time the myosin is moving. The image obtained represents the average position of the myosin during that frame. Velocities are calculated using the time interval between the midpoint of each frame. The final output from the program is a file containing the run length and speed for each trajectory. The run lengths were then combined into a histogram with bin size of 0.2 μm. For WT and Y-Loop2, the minimum bin started at 0.5 μm, whereas for Y-MD the minimum bin started at 0.8 μm. This minimum corresponds approximately to the distance over which each construct moves in four frames, and the minimum bin is higher for Y-MD because it moves with a higher velocity than the other two constructs. The run length distribution histogram was fit with

$$p(x) = Ae^{-x/\lambda} \qquad \text{(Eq. 1)}$$

to determine the characteristic run length λ where $p(x)$ is the probability of the myosin traveling a distance x along an actin filament and A is a constant.

Our characteristic run lengths for WT are shorter than those reported by Baker *et al.* (18) ($\lambda \sim 1$ μm for WT in 25 mM KCl). A major difference is that the earlier data were analyzed by hand, whereas we used an automated tracking program. The automated program tends to result in shorter run lengths because it is better at detecting short runs than humans and because the YFP fluorescence emission occasionally flickers. If the fluorescence intensity flickers in the middle of a run, the tracking program will occasionally count this as two short runs, whereas a human analyzing the data will count this as one long run.

In Vitro Motility—Ensemble motility assays were performed essentially as described previously (16). For the standard motility assays, the myosin was diluted to 25 or 50 μg/ml and adsorbed directly to nitrocellulose-coated coverslips that were preincubated with 0.01 mg/ml bovine serum albumin for 30 s (2). The motility assay was performed at 30 °C in Motility Buffer with 25–100 mM KCl and 2 mM MgATP. Filament velocities were calculated using the program described by Work and Warshaw (19).

Landing Rates—Actin filament landing rates were used to test the processivity of WT and Y-Loop2 (20). The landing rate R depends on the myosin density ρ according to

$$R(\rho) = Z(1 - e^{-\rho/\rho_0})^n \qquad \text{(Eq. 2)}$$

where n is the number of myosin molecules required to move the actin filament, ρ_0 reflects the average surface area over which myosin can interact with an actin filament, and Z depends on the collision rate and the affinity of myosin for actin (21). An anti-YFP antibody (3E6 mAb, Qbiogene, Inc.) was used to attach the myosin to the nitrocellulose-coated coverslip. The flow cell was prepared by incubating it with 20 μg/ml antibody for 2 min, blocking with 1.0 mg/ml bovine serum albumin for 2 min, and finally incubating with varying concentrations of myosin for 2 min. The landing rate buffer was Motility Buffer with 25 or 100 mM KCl, 2 mM MgATP, 0.5 mg/ml bovine serum albumin, and 40 nM (for WT and Y-Loop2 in 25 mM KCl) or 80 nM (for Y-Loop2 in 100 mM KCl) phalloidin-rhodamine-labeled actin. The labeled actin was sheared by passing it through a 22.5-gauge needle five times. This assay was performed in the TIRF setup described above at 25 ± 1 °C. The rhodamine-labeled actin was excited with the 514-nm line of the argon laser, and the emission filter was a Chroma HQ 575/60. The data were collected at 8 frames/s, and the pixel resolution was 21.5 nm. To qualify as a landing event, an actin filament had to attach to the surface and move smoothly for at least 0.2 μm over at least four frames. The myosin surface density was calculated by assuming that all the myosin bound equally to the top and bottom surfaces and all the adsorbed molecules were fully functional.

Landing Rate Analysis—The data were fit to Equation 2. None of the three parameters (Z, ρ_0, and n) were fixed; all were determined by the fit. A processive motor by definition should have a value of $n = 1$, and this has been observed for strongly processive motors such as kinesin and wild type myosin V (2, 21). Our result for Y-Loop2 in 25 mM KCl was $n = 2.1$, and yet we interpreted this to be a processive motor. The

discrepancy lies in the fact that Y-Loop2 is only weakly processive. In the derivation of Equation 2, n is the number of motors attached to the actin filament at any given time. We required that an actin filament move at least 0.2 μm after attaching to the surface to qualify as a landing event to distinguish between real events and diffusion. This is equivalent to 5.6 steps where each step is 36 nm. The characteristic TIRF run length for Y-Loop2 under these conditions was only 0.27 μm (7.5 steps). This implies that close to half of the filaments that actually landed and attached to a single myosin would have detached before reaching the 0.2-μm cutoff, thus reducing the number of events. This effect is most severe at low myosin densities when actin is most likely to be attached to a single myosin, leading to a steeper dependence of the landing rate on myosin density and thus a higher n value. To our knowledge this is the first time a landing rate assay has been performed on a weakly processive motor.

Steady-state Actin-activated ATPases—Actin-activated ATPase assays were performed at 37 °C in 10 mM imidazole, pH 7.4, 50 mM KCl, 1 mM MgCl$_2$, 1 mM DTT, 1 mM EGTA, 2 mM MgATP, and 12 μM exogenous CaMΔall. The buffers also contained an ATP-regenerating system (0.2 mM NADH, 0.5 mM phosphoenolpyruvate, 20 units/ml lactate dehydrogenase, 100 units/ml pyruvate kinase). The rate of the reaction was measured from the decrease in absorbance at 340 nm caused by the oxidation of NADH by lactate dehydrogenase. This assay minimizes the time-dependent ADP-induced inhibition of actin-activated ATPase activity. For each actin concentration, data from three separate assays with at least two different preparations of each construct were combined to find average ATPase rates. Data were then fitted to the Michaelis-Menten equation to obtain the maximum ATPase rate (V_{max}) and K_m.

RESULTS

Expressed Constructs—A WT murine myosin V HMM and two chimeric constructs were expressed using the baculovirus/insect cell system (Fig. 1). YFP was cloned at the C terminus of the heavy chain to serve as the fluorophore for single molecule studies. The chimeric constructs Y-MD and Y-Loop2 contained elements of both murine myosin V and Myo4p, the non-processive class V myosin from yeast (11). Y-MD contains the entire yeast motor domain, whereas Y-Loop2 contains only loop 2 from yeast. Both chimeras contained the neck and rod of WT-HMM.

Maximal Actin-activated ATPase Rate Correlates with Motility—The actin-activated ATPase of the three constructs was determined in 50 mM KCl with an ATP-regenerating system to prevent inhibition by ADP (Fig. 2a). The maximal ATPase rate per head was much higher for Y-MD than for either WT or Y-Loop2 (V_{max} values of 26.8 ± 3.1, 12.3 ± 0.5, and 9.5 ± 0.3 s^{-1}, respectively). Loop 2 therefore does not have a substantial effect on the maximal ATPase rate, but it does affect its apparent affinity for actin in the presence of MgATP as assessed by the K_m values. The order of apparent affinity for actin was WT-HMM >

FIGURE 1. *a*, schematic of the constructs. WT is an HMM-like fragment of dilute mouse myosin V. The other two constructs are chimeras of mouse (*red*) and yeast (*blue*) myosin V. Y-Loop2 contains loop 2 from yeast, whereas Y-MD contains the entire yeast motor domain. All constructs have YFP at the C terminus of the heavy chain. *b*, comparison of mouse and yeast loop 2 sequences.

FIGURE 2. **ATPase and motility assays.** *a*, actin-activated ATPase assays for WT (*red squares*), Y-Loop2 (*blue circles*), and Y-MD (*green triangles*). V_{max} and K_m values were 12.3 ± 0.5 s^{-1} and 2.8 ± 0.4 μM for WT, 9.5 ± 0.3 s^{-1} and 10.0 ± 0.7 μM for Y-Loop2, and 26.8 ± 3.1 s^{-1} and 30.3 ± 5.7 μM for Y-MD, respectively. Values are averages ± S.D. of at least three different assays with two different preparations of each construct. Conditions were as follows: 37 °C, 50 mM KCl, 2 mM MgATP. *b*, actin filament sliding speed measured in the ensemble *in vitro* motility assay. Values are averages ± S.D. for at least 80 filaments and at least two preparations of each construct. Conditions were as follows: 30 °C, 50 mM KCl, 2 mM MgATP.

TABLE 1
Summary of ATPase, motility, and ionic strength dependence of run length

Construct	Loop 2	Motor domain	V_{max}	K_m	Speed from motility	Run length dependence on ionic strength
			s^{-1}	μM	$\mu m/s$	
WT	Mouse	Mouse	12.3 ± 0.5	2.8 ± 0.4	0.36 ± 0.03	Low
Y-Loop2	Yeast	Mouse	9.5 ± 0.3	10.0 ± 0.7	0.38 ± 0.04	High
Y-MD	Yeast	Yeast	26.8 ± 3.1	30.3 ± 5.7	1.41 ± 0.11	High
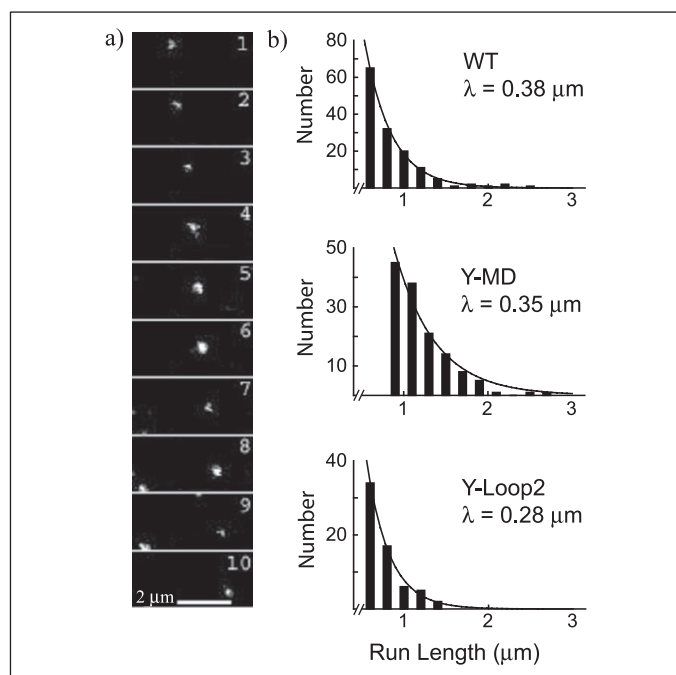
FIGURE 3. **Single molecule processive runs.** *a*, TIRF microscopy image sequence shows a Y-Loop2 molecule moving processively along an actin filament (filament not visible). The time interval between each image is 0.3 s. The *scale bar* is 2 μm. *b*, run length data for WT, Y-MD, and Y-Loop2. The *curve* in each histogram is a fit to the equation $y = Ae^{-x/\lambda}$ where λ is the characteristic run length for each construct. Conditions were as follows: 25 °C, 50 mM KCl, 50 μM MgATP.

FIGURE 4. **Processive run lengths and velocities from single molecule data.** *a*, the characteristic run length from the TIRF microscopy assay for WT (*red squares*), Y-Loop2 (*blue circles*), and Y-MD (*green triangles*) as a function of KCl concentration. *b*, speed of single myosin Vs during a processive run as a function of KCl concentration. Symbols are the same as in *a*. The velocity and run length for Y-Loop2 in 100 mM KCl were not determined because the construct was not processive under these conditions. Conditions were as follows: 25 °C, varying KCl, 50 μM MgATP.

Y-Loop2 > Y-MD (K_m values of 2.8 ± 0.4, 10.0 ± 0.7, and 30.3 ± 5.7 μM, respectively). Although we use K_m as a measure of the apparent affinity of actin for myosin, the situation is more complicated for a processive than a non-processive myosin (see "Discussion" for more detail).

In vitro motility assays were also performed on each construct at 50 mM KCl (Fig. 2*b*). The actin filament sliding speed of each construct showed the same pattern as the maximal ATPase rate (Table 1). The speeds of WT and Y-Loop2 were nearly identical (0.36 ± 0.03 and 0.38 ± 0.04 μm/s, respectively), whereas Y-MD was much faster (1.41 ± 0.11 μm/s). The maximum actin filament sliding speed of native yeast myosin V (Myo4p) was reported to be 1.1 μm/s (11), similar to the value seen here for Y-MD.

Single Molecule Processive Run Lengths—TIRF microscopy was used to directly test the processivity of the three constructs. Actin filaments are bound to a coverslip, and YFP-labeled HMM in solution can attach to the actin filament, move processively along it, then detach, and go back into solution. A typical image sequence of a YFP-HMM moving along a surface-bound actin filament as a function of time is shown in Fig. 3*a*. Both the run length distribution and the velocity can be calculated from these data. The run length distribution for WT, Y-MD, and Y-Loop2 in 50 mM KCl is shown in Fig. 3*b.* For each distribution, the *solid line* shows an exponential fit with a characteristic run length λ, which represents the average length a myosin molecule travels along an actin filament before dissociating.

Given that yeast Myo4p has been reported to be a non-processive motor (11), we were surprised to observe that Y-MD was processive by this direct assay with a characteristic run length similar to that of WT at 50 mM KCl ($\lambda = 0.35$ μm for Y-MD *versus* $\lambda = 0.38$ μm for WT). Y-Loop2 was slightly less processive than WT ($\lambda = 0.28$ μm). The processivity of each construct was tested at several KCl concentrations to determine whether this trend persisted (Fig. 4*a*). The run length for WT was nearly independent of salt concentration from 25 to 100 mM KCl. In contrast, the characteristic run length for both chimeras depended strongly on KCl concentration. Y-MD had longer characteristic run lengths than WT at low salt concentrations but shorter run lengths at high KCl. Y-Loop2 was processive at low ionic strength with run lengths gradually decreasing with ionic strength until it was non-processive in 100 mM KCl. The feature common to Y-Loop2 and Y-MD is the yeast loop 2 sequence, implying that this region is responsible for their similar ionic strength dependence.

The speed at which the single molecules moved during a processive run along actin was also calculated from the TIRF microscopy data (Fig. 4*b*). The velocity of WT and Y-Loop2 was similar and fairly constant as a function of salt. In agreement with this observation, ADP release rates from WT were nearly invariant from 25 to 100 mM KCl (data not shown). In contrast, Y-MD was faster than either of these constructs, and the speed showed more of an ionic strength dependence.

Landing Rate Assays—When no processive runs are observed by TIRF microscopy, an independent assay is necessary to establish that a
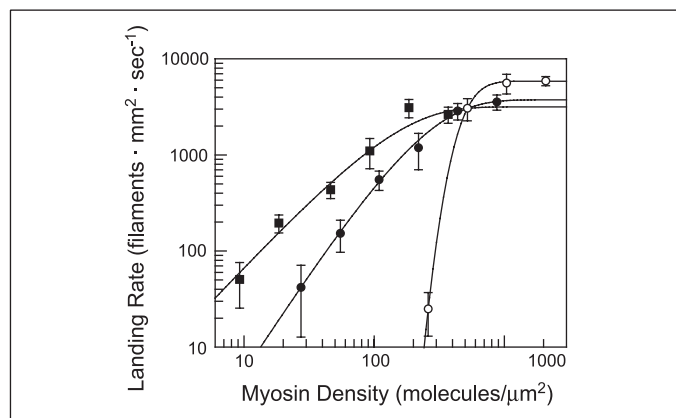
FIGURE 5. **Landing rate assays.** Dependence of actin filament landing rate on myosin surface density for WT in 25 mM KCl (■), Y-Loop2 in 25 mM KCl (●), and Y-Loop2 in 100 mM KCl (○) is shown. Equation 2 was fit to each data set, yielding $n = 1.4 \pm 0.4$ for WT (25 mM KCl), $n = 2.1 \pm 0.2$ for Y-Loop2 (25 mM KCl), and $n = 40.3 \pm 4.2$ for Y-Loop2 (100 mM KCl).

construct is not processive. The actin filament landing rate was measured as a function of myosin surface density for Y-Loop2 at two ionic strengths and for WT as a control (Fig. 5). The data at each condition were fit to Equation 2 (see "Materials and Methods") to obtain a value of n, the number of myosin molecules required to move an actin filament. The behavior of both constructs was similar in 25 mM KCl with $n = 1.4 \pm 0.4$ for WT and $n = 2.1 \pm 0.2$ for Y-Loop2. Although $n = 1$ is usually observed for strongly processive motors (2, 21), this is the first time a landing rate assay has been performed on a weakly processive motor. We interpreted these results to indicate that both WT and Y-Loop2 are processive in 25 mM KCl, although Y-Loop2 is only weakly processive (see "Materials and Methods" for a more detailed discussion). This is in agreement with the single molecule TIRF measurements. As additional evidence for processivity, at low myosin densities filaments were observed to swivel about a single attachment point as they moved, implying movement by a single myosin motor.

In contrast, Y-Loop2 was highly non-processive in 100 mM KCl ($n = 40.3 \pm 4.2$). No landing events were observed at myosin densities of 130 molecules/μm^2 or less, and no filaments were observed to swivel about a single point. These observations indicate that multiple motors were required to move filaments, also in agreement with the lack of processive runs observed by single molecule TIRF measurements.

DISCUSSION

Our chimeric constructs revealed several features about myosin V processivity. We showed that the yeast Myo4p motor domain is capable of supporting processive movement. We also found that loop 2 plays an important role in determining processive run lengths in agreement with structural data that show that loop 2 tethers myosin V to actin in the ATP and transition states (22). A highly positively charged loop 2 appears to be important for maintaining processivity, particularly near physiologic ionic strength. Wild-type mouse myosin V remained highly processive over a range of salt concentrations, whereas the processive run lengths of chimeras containing yeast loop 2 decreased sharply as the salt concentration was increased. Two models, which differ in whether loop 2 affects an attachment or a detachment step, were used to interpret these data.

The Yeast Class V Myosin Motor Domain Supports Processive Movement

Class V myosins isolated from yeast (Myo2p and Myo4p) have been reported to be low duty ratio, non-processive motors based on motility

and landing rate assays and to have a low affinity for actin in the presence of ATP (11). Surprisingly we found that the chimera containing the entire motor domain from yeast myosin V (Myo4p) and the neck and rod from murine myosin V was highly processive with longer run lengths than WT murine myosin V at low ionic strength. Our results establish that the yeast Myo4p motor domain has all the kinetic and structural properties necessary to support processive movement.

There are several possible explanations for the difference in processivity between native yeast myosin V and Y-MD. The most interesting possibility is that the native rod region of Myo4p does not form a stable coiled-coil, and thus the molecule can exist as either a monomer (non-processive) or a dimer (processive), depending on conditions. This possibility is based on a Paircoil analysis of the rod sequence of yeast Myo4p that shows only five heptad repeats of potential coiled-coil. This hypothesis is currently being tested with additional expressed constructs containing the yeast rod region. A monomer-dimer equilibrium that impacts on processivity has recently been proposed to exist with class VI myosins (for a review, see Ref. 23), and it is possible that this may be a general mechanism for regulating processivity *in vivo*.

An alternative possibility is that the study of Reck-Peterson *et al.* (11) inferred a lack of processivity because of indirect assays and the limited conditions. Their experiments were performed at 75 mM KCl and 10 mM MgATP, which corresponds to a relatively high ionic strength of $\sim$147 mM. It is possible that native yeast Myo4p is non-processive (or weakly processive) at this high ionic strength and more processive at lower ionic strength. This possibility is suggested by our experiments in which Y-MD was only weakly processive in 100 mM KCl (ionic strength = 137 mM). A direct single molecule processivity assay as a function of ionic strength needs to be performed with the native yeast myosin Vs.

A High Affinity for Actin Is Important for Processivity

A unique feature of vertebrate myosin Vs is that their affinity for actin in the ATP and ADP·P$_i$ states is higher than that of most other myosins, implying that this may be a characteristic that influences processivity (8). Loop 2, a surface loop involved in the initial weak electrostatic interaction with actin, affects the affinity of myosin for actin in the presence of MgATP. Because positive charges in loop 2 interact with acidic patches on actin, increasing the net positive charge of the loop results in a higher affinity for actin (13, 14) without affecting other steps in the catalytic cycle of myosin V (15).

The mouse and yeast motor domains are 47% identical and 69% similar, but there are regions, including loop 2, where the differences are clustered (Fig. 1*b*). Yeast loop 2 is shorter than mouse loop 2 (31 *versus* 41 residues) and has a different charge distribution. The net charge of the mouse loop is +6 (+9, −3), whereas the yeast loop has no net charge (+6, −6), and all of its six negative charges are located in the first half of the loop. The overall electrostatic interaction with actin should be much weaker for yeast than for murine loop 2, resulting in lower actin affinities. Our ATPase data showed that exchanging the yeast loop 2 into the mouse motor domain decreased the apparent affinity for actin in the presence of MgATP by 3-fold, but it did not affect ensemble motility rates, the maximal actin-activated ATPase rate, or velocities of single molecules during a processive run. Y-Loop2 showed reduced run lengths relative to WT under all conditions tested, especially at 100 mM KCl where the molecule was completely non-processive. From this we conclude that a high affinity for actin in the presence of ATP is important for processive movement.

Structural data in support for this statement were obtained by electron cryomicroscopy of actin decorated with murine myosin V (22). In

the presence of ATP, the long cleft that divides the motor domain opens, leading to a reduced affinity for actin. To compensate for this reduced affinity caused by disruption of the strong binding actomyosin interface, loop 2 rearranges on actin to act as a tether to maintain proximity of actin and myosin primarily via electrostatic interactions with acidic patches on actin. The loop from yeast will have less tendency to act as a tether compared with the more positively charged loop 2 derived from mouse.

Loop 2 Determines the Ionic Strength Dependence of Processive Run Lengths

The presence of yeast loop 2, in either Y-Loop2 or Y-MD, caused processive run lengths to decrease as the ionic strength was increased. The trend observed for the two constructs was quite similar (Fig. 4*a*). In contrast, the characteristic run length of WT decreased only slightly over this same range of salt (25–100 mM KCl). Loop 2 therefore is a primary determinant of the ionic strength dependence of run lengths.

The yeast loop 2 is net neutral, but there are a total of six negative and six positive charges, which occur in clusters of like charge. The interaction between loop 2 and subdomain 1 of actin is electrostatic (13–15). As ionic strength is increased, the interaction between loop 2 and actin is screened, resulting in a lower affinity for actin. For Y-MD and Y-Loop2, this results in shorter run lengths as the ionic strength is increased. Because the mouse loop 2 in WT has a higher net charge than that of the yeast loop 2, one would expect the run lengths of WT to show a stronger ionic strength dependence. However, because loop 2 is long and unstructured, the interaction with subdomain 1 of actin is more complicated than a simple charge-charge interaction and will depend on the exact charge distribution of the loop. We speculate that there is a critical interaction strength necessary for high processivity and that this critical level is attained by the mouse loop 2 but not the yeast loop 2.

Attachment Rates to Actin

Attachment rates of the various constructs to actin can be estimated in several ways. The K_m from the steady-state ATPase data is a good approximation of the "apparent" affinity for actin for a non-processive myosin or single headed myosin V (24). However, the situation is more complicated for a processive myosin, which can take multiple steps each time it encounters an actin filament. Whether or not this actually occurs at the high actin concentrations used in the steady-state ATPase is unclear. Assuming that the double headed molecule is not walking processively during an ATPase assay and that each myosin head hydrolyzes only one ATP per encounter with actin, then

$$K_m \approx k_{\text{ATPase}}/k_{\text{on}} \qquad \text{(Eq. 3)}$$

where k_{ATPase} is the ATPase activity and k_{on} is the second order rate constant for binding of myosin to actin in the presence of ATP (25). This approximation assumes that reverse rate constants are zero, but the result is similar if we take into account the fact that ATP hydrolysis is not irreversible (24). Using V_{max} for k_{ATPase}, k_{on} was calculated to be 4.4 $\mu\text{M}^{-1}\,\text{s}^{-1}$ for WT, 0.95 $\mu\text{M}^{-1}\,\text{s}^{-1}$ for Y-Loop2, and 0.88 $\mu\text{M}^{-1}\,\text{s}^{-1}$ for Y-MD. This analysis suggests that the attachment rates for Y-Loop2 and Y-MD are ≈5 times slower than for WT. The value for WT agrees well with the published result of 4.7 $\mu\text{M}^{-1}\,\text{s}^{-1}$ for chicken myosin V (26).

Alternatively if myosin is walking processively along actin filaments in the ATPase assay, then we can use the approximation,

$$K_m \approx K_d = k_{\text{off}}/k_{\text{on}} \qquad \text{(Eq. 4)}$$

to calculate k_{on}. Single molecule processive runs are used to calculate $k_{\text{off}} = 1/t_{\text{attached}}$. The average time that myosin spends on the actin filament (t_{attached}) is obtained from the average run length and velocity. The resulting attachment rates were 0.42 $\mu\text{M}^{-1}\,\text{s}^{-1}$ for WT, 0.17 $\mu\text{M}^{-1}\,\text{s}^{-1}$ for Y-Loop2, and 0.067 $\mu\text{M}^{-1}\,\text{s}^{-1}$ for Y-MD. Either approach suggests that attachment rates are higher for WT and that the primary effect of loop 2 on processivity is on the rate at which the detached head reattaches to the actin filament during processive stepping.

How Does Actin Affinity Affect Processivity?

Model 1—The most intuitive idea is that the state vulnerable to termination is one in which a single head is bound to actin while the other head is detached, undergoing a diffusive search for the next actin binding site. A lower affinity for actin would decrease the rate at which the detached head reattaches to actin. In this model, myosin V starts with both heads bound in the ADP state (Fig. 6*a*). The rear head detaches from actin and swings forward with rate k_{step}, which is essentially the ATPase rate. This is determined by two steps, ADP release and ATP binding to the rear head. The processive run length is determined by a competition between the rate at which the detached head reattaches to actin (k_{reattach}) and the rate at which the attached head dissociates from the actin filament (k_{term}). Following a model similar to that of Rosenfeld and Sweeney (6), k_{term} is the rate at which ADP is released from the attached head. As soon as ADP is released from the attached head, ATP binds, and it dissociates. The detached head must reattach to actin before this happens for the processive run to continue. The run length from this scheme is as follows.

$$\lambda = 36 \text{ nm} \times \left(1 + \frac{k_{\text{reattach}}}{k_{\text{term}}}\right) \qquad \text{(Eq. 5)}$$

We calculate k_{step}, the rate at which the molecule takes a step, from the single molecule velocity (assuming 36-nm steps). We then assume that $k_{\text{term}} \approx k_{\text{step}}$. The unstrained ADP release rate from the singly attached head is assumed to be equal to the ADP release rate from the rear head when both heads are attached. This is an approximation because intramolecular strain may accelerate ADP release from the rear head (4–6), although this view is not universally accepted (7). The experimentally measured characteristic run lengths are then used to calculate k_{reattach} using Equation 5 (Fig. 6*b*).

The calculated k_{reattach} for Y-Loop2 is slower than that for WT at all salt concentrations. Thus WT is more processive than Y-Loop2 because the reduced charge in the yeast loop 2 leads to slower reattachment rates for the detached head. This model can also account for the salt dependence of both Y-Loop2 and Y-MD. As the salt concentration is increased, the electrostatic interaction between loop 2 and actin is screened, and k_{reattach} decreases.

This model does not explain the lack of salt dependence of WT or the fast reattachment rates for Y-MD at low salt. These latter two discrepancies can be explained if we assume that the reattachment of the front head occurs in two steps. The first step is the diffusive search of the lead head for the next actin binding site and the subsequent rebinding, which will depend on the net charge of loop 2. The next step is phosphate release, which is unaffected by loop 2 (15). Assuming that phosphate release precedes the weak to strong binding transition, myosin is vulnerable to termination until phosphate is released from the front head. A high actin affinity will also stabilize the weakly bound front head until phosphate is released. If the rebinding step is fast compared with phosphate release, then this is the termination pathway proposed by Rosenfeld and Sweeney (6). The phosphate release rate was reported to be ≈100–230 s^{-1} for chicken myosin V (6, 15), similar to k_{reattach} for WT. Thus one explanation for the lack of salt dependence in WT is that the
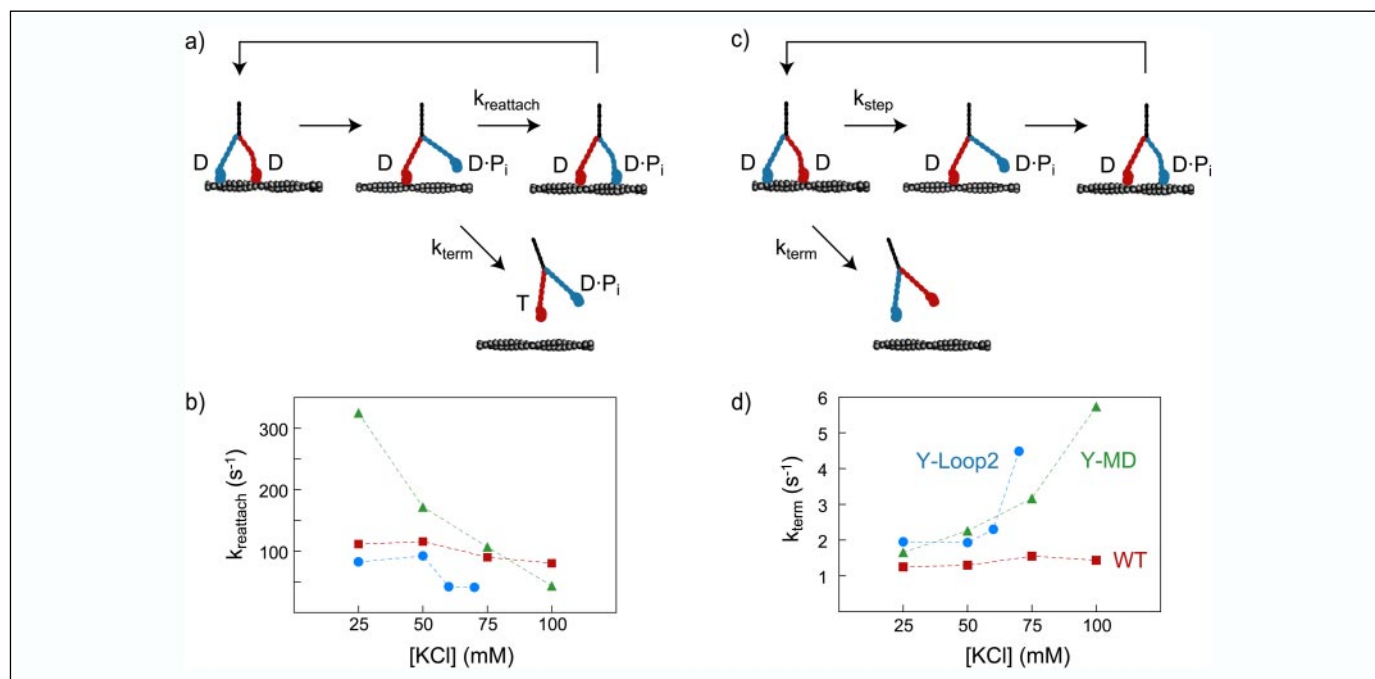
FIGURE 6. **Two models for how actin affinity affects processivity.** *a*, model 1 scheme. Run lengths are determined by a competition between the rate at which the detached head reattaches to actin (k_{reattach}) and the rate at which the single attached head dissociates from actin (k_{term}). *b*, k_{reattach} as a function of salt concentration calculated from model 1 (Equation 5) for WT (*red squares*), Y-Loop2 (*blue circles*), and Y-MD (*green triangles*). *c*, model 2 scheme. Run lengths are determined by a competition between the rate at which myosin takes a step (k_{step}) and the rate at which it dissociates from actin from a state in which both heads are bound (k_{term}). The nucleotide state of the dissociated myosin is left blank because there is more than one possibility. *d*, k_{term} calculated from model 2 (Equation 6) as a function of salt concentration. In these simple models, one rate might represent several substeps, *e.g.* k_{step} represents ADP release from the rear head followed by ATP binding, dissociation of the head, and ATP hydrolysis. *T*, ATP; *D*, ADP.

rebinding step is fast for all salt concentrations tested, and k_{reattach} is essentially the phosphate release rate. In contrast, for Y-Loop2 and Y-MD, the lower affinity for actin decreases the rate of rebinding, which becomes similar to or slower than the phosphate release rate. Thus increased ionic strength decreases k_{reattach}. If the phosphate release rate is higher for Y-MD than for WT and Y-Loop2, this would also explain the high k_{reattach} for Y-MD at low salt.

Model 2—In model 2, we consider the possibility that loop 2 affects processive run lengths by affecting the rate at which myosin dissociates from actin as opposed to affecting the attachment rate. Here the reattachment step is assumed to be fast so that a processive run does not terminate from a state with one head bound. Instead runs terminate from a state in which both heads are bound to actin at rate k_{term}. Because myosin V spends most of its time in this state, run lengths are maximized by taking as many steps as possible in a given time. The run length is then determined by a competition between the ATPase rate (k_{step}) and the termination rate (k_{term}) (Fig. 6*c*). The characteristic run length from this model is as follows.

$$\lambda = 36 \text{ nm} \times \left(1 + \frac{k_{\text{step}}}{k_{\text{term}}}\right) \qquad \text{(Eq. 6)}$$

In this model, a higher ATPase rate results in longer run lengths, whereas higher termination rates result in shorter run lengths. We calculated k_{step} from the single molecule velocity data (assuming 36-nm steps) and along with the experimentally measured run lengths used Equation 6 to calculate the termination rates (Fig. 6*d*). WT had termination rates of about 1.4 s^{-1}, nearly independent of salt concentration. In contrast, the termination rates for Y-MD and Y-Loop2 increased dramatically at high salt. WT is more processive than Y-Loop2 because it has lower termination rates and similar ATPase rates. Y-MD is more processive than Y-Loop2 because it has higher ATPase rates and similar

termination rates. Y-MD is more processive at low ionic strength than WT because it has a higher ATPase rate and similar termination rate. At high ionic strength the fast termination rates dominate for Y-MD, and it becomes less processive than WT.

Although it seems unlikely that myosin V would dissociate from a state in which both heads are bound to actin in the ADP state, it was shown recently that a single headed myosin V construct under rearward strain dissociates from actin at a rate of 1.5 s^{-1} (7). The authors proposed that myosin dissociates from a weakly bound ADP state, a situation that occurs in the lead head of a doubly bound myosin V under intramolecular strain. Our calculated termination rate of 1.4 s^{-1} for WT is nearly the same as the dissociation rate measured by Purcell *et al.* (7). Thus we speculate that termination of a processive run might occur when the front head dissociates from actin before the rear head. After the front head dissociates, the rear head will then dissociate upon loss of ADP and binding of ATP. For Y-Loop2 and Y-MD, the "weaker" loop 2 results in a higher dissociation rate for the front head.

Comparison of the Two Models—In model 1, the primary effect of loop 2 is on the reattachment step, which is supported by structural data (22) and by the higher reattachment rates for WT calculated from steady-state ATPase data. If the reattachment step includes phosphate release, then this model can also account for the lack of salt dependence for WT and the high reattachment rates for Y-MD. In model 2, the primary effect of loop 2 is on the rate at which doubly bound myosin dissociates from actin. This model is supported by kinetic data showing that reducing the net charge of loop 2 reduces the affinity of myosin for actin in all nucleotide states (15). This model attributes the high processivity of Y-MD at low ionic strength to its high ATPase rate and explains most of the data well except for the lack of salt dependence of WT. More kinetic data would be necessary to distinguish between the two models and to design a more complicated model.

Myosin V Processivity

REFERENCES

1. Reck-Peterson, S. L., Provance, D. W., Jr., Mooseker, M. S., and Mercer, J. A. (2000) *Biochim. Biophys. Acta* **1496,** 36–51
2. Mehta, A. D., Rock, R. S., Rief, M., Spudich, J. A., Mooseker, M. S., and Cheney, R. E. (1999) *Nature* **400,** 590–593
3. De La Cruz, E. M., and Ostap, E. M. (2004) *Curr. Opin. Cell Biol.* **16,** 61–67
4. Veigel, C., Wang, F., Bartoo, M. L., Sellers, J. R., and Molloy, J. E. (2002) *Nat. Cell Biol.* **4,** 59–65
5. Veigel, C., Schmitz, S., Wang, F., and Sellers, J. R. (2005) *Nat. Cell Biol.* **7,** 861–869
6. Rosenfeld, S. S., and Sweeney, H. L. (2004) *J. Biol. Chem.* **279,** 40100–40111
7. Purcell, T. J., Sweeney, H. L., and Spudich, J. A. (2005) *Proc. Natl. Acad. Sci. U. S. A.* **102,** 13873–13878
8. Yengo, C. M., De la Cruz, E. M., Safer, D., Ostap, E. M., and Sweeney, H. L. (2002) *Biochemistry* **41,** 8508–8517
9. Vale, R. D. (2003) *J. Cell Biol.* **163,** 445–450
10. Toth, J., Kovacs, M., Wang, F., Nyitray, L., and Sellers, J. R. (2005) *J. Biol. Chem.* **280,** 30594–30603
11. Reck-Peterson, S. L., Tyska, M. J., Novick, P. J., and Mooseker, M. S. (2001) *J. Cell Biol.* **153,** 1121–1126
12. Spudich, J. A. (1994) *Nature* **372,** 515–518
13. Furch, M., Geeves, M. A., and Manstein, D. J. (1998) *Biochemistry* **37,** 6317–6326
14. Joel, P. B., Sweeney, H. L., and Trybus, K. M. (2003) *Biochemistry* **42,** 9160–9166
15. Yengo, C. M., and Sweeney, H. L. (2004) *Biochemistry* **43,** 2605–2612
16. Krementsov, D. N., Krementsova, E. B., and Trybus, K. M. (2004) *J. Cell Biol.* **164,** 877–886
17. Pardee, J. D., and Spudich, J. A. (1982) *Methods Enzymol.* **85,** 164–181
18. Baker, J. E., Krementsova, E. B., Kennedy, G. G., Armstrong, A., Trybus, K. M., and Warshaw, D. M. (2004) *Proc. Natl. Acad. Sci. U. S. A.* **101,** 5542–5546
19. Work, S. S., and Warshaw, D. M. (1992) *Anal. Biochem.* **202,** 275–285
20. Howard, J., Hudspeth, A. J., and Vale, R. D. (1989) *Nature* **342,** 154–158
21. Hancock, W. O., and Howard, J. (1998) *J. Cell Biol.* **140,** 1395–1405
22. Volkmann, N., Liu, H., Hazelwood, L., Krementsova, E. B., Lowey, S., Trybus, K. M., and Hanein, D. (2005) *Mol. Cell* **19,** 595–605
23. Buss, F., Spudich, G., and Kendrick-Jones, J. (2004) *Annu. Rev. Cell Dev. Biol.* **20,** 649–676
24. De La Cruz, E. M., Wells, A. L., Sweeney, H. L., and Ostap, E. M. (2000) *Biochemistry* **39,** 14196–14202
25. Howard, J. (2001) *Mechanics of Motor Proteins and the Cytoskeleton*, p. 95, Sinauer Associates, Sunderland, MA
26. De La Cruz, E. M., Wells, A. L., Rosenfeld, S. S., Ostap, E. M., and Sweeney, H. L. (1999) *Proc. Natl. Acad. Sci. U. S. A.* **96,** 13726–13731